Design and development of layer-by-layer based low-pressure antifouling nanofiltration membrane used for water reclamation

Xin Li[a], Chang Liu[a], Wenqiang Yin[a, b], Tzyy Haur Chong[a, b], Rong Wang[a, b, *]

[a] Singapore Membrane Technology Centre, Nanyang Environment and Water Research Institute, Nanyang Technological University, 1 Cleantech Loop, Singapore 637141, Singapore

[b] School of Civil and Environmental Engineering, Nanyang Technological University, 50 Nanyang Avenue, Singapore 639798, Singapore

* Corresponding author at: School of Civil and Environmental Engineering, Nanyang Technological University, 50 Nanyang Avenue, Singapore 639798, Singapore.
Tel.: +65 6790 5327; fax: +65 6791 0676.
E-mail address: rwang@ntu.edu.sg (R. Wang)

Abstract:

Recent studies have confirmed the advantages of low-pressure nanofiltration (NF) membranes in integrated nanofiltration membrane bioreactor system followed by the reverse osmosis (RO) process for high recovery water reclamation. However, fouling of low-pressure NF membranes restricts their application in providing high quality feed to subsequent RO process. In this study, an antifouling low-pressure NF membrane was designed and fabricated via rapid co-deposition of polydopamine (PDA)/polyethylenimine (PEI) on electrostatic layer-by-layer (LBL) assembled polyethersulfone (PES) flat sheet membrane followed by crosslinking with glutaraldehyde. The optimized resultant membrane (LBL-cPP) presented approximately 11 LMH/bar pure water permeability with more than 90% rejection divalent cations under 2 bar pressure. The newly developed selective layer exhibited excellent antifouling performance and chemical stability ascribing to the inherent hydrophilicity of PDA/PEI and dual covalent reaction of PDA with the LBL layer. By feeding real municipal wastewater, the LBL-cPP membrane also achieved superior permeate quality, leading to lower RO fouling rate in subsequent RO unit as compared to commercial NF 270 membrane. Further organic foulant analysis indicated that 96.8% of dissolved organic carbons were effectively removed by the LBL-cPP membrane. Specifically, the novel NF membrane demonstrated high removal rate (> 93%) for foulants with low molecular weights which was largely responsible for RO fouling, while maintaining the desired flux recovery rate and reduced cleaning frequency. This study demonstrates the potential of PDA/PEI modified low-pressure NF membranes in designing efficient and sustainable water reclamation technology.

Keywords: Polydopamine; Layer-by-layer; Nanofiltration; Membrane fouling; Water reclamation.

1. Introduction

Rapid urbanization creates enormous pressure on water use and infrastructure, which makes

water an increasingly limited resource worldwide [1, 2]. To address the challenge, there is an urgent need to develop advanced water reclamation technologies for tapping unconventional water sources to augment water supply. The benefits brought by water reclamation are not only to reduce the requirement for high quality tap water but also to alleviate water pollution by controlling wastewater discharge into natural water bodies [3].

The rational selection of various treatment technologies for water reclamation is dependent on the intended use of treated water and other factors such as cost, energy demands, and apposite space for treatment plants. Among various options, membrane bioreactor (MBR) integrated with reverse osmosis (RO) process has attracted much attention [4, 5]. Compared to conventional activated sludge (AS) treatment, MBR is more robust, versatile, and able to produce effluent of higher standard with less sludge production and smaller physical footprint [6]. Moreover, the feasible incorporation of MBR and RO demonstrates a better coherent foulant removal ability and reduced fouling rate than traditional AS + microfiltration/ultrafiltration + RO processes for water reclamation. However, in conventional MBR + RO system, although high recovery levels (75-85%) of RO can be achieved by using two or more stages of RO, the practical recovery is still limited by RO membrane fouling that leads to compromised production efficiency and raised energy consumption [7, 8]. One effective strategy to mitigate RO fouling is to improve the quality of RO feed by integrating nanofiltration (NF) with biological reactor to form the NF-MBR configuration [9, 10]. NF-MBR + RO performs better and is more feasible than UF-MBR + RO, ascribing to the contributions of NF: (i) effective removal of divalent ions and most organic compounds, especially those with low molecular weights, by means of size exclusion and electrostatic repulsion; (ii) low monovalent salt rejection, thus reducing salt accumulation in the bioreactor; (iii) compact design. However, NF-MBR for wastewater treatment is still at the nascent stage, limited mainly by the low permeability or high operational pressure required for the NF process. As a result, the development of highly energy-efficient NF membrane with effective removal of organic compounds and divalent salts as well as anti-fouling property is paramount for water reclamation application.

The layer-by-layer (LBL) electrostatic assembly method is an effective approach for

synthesizing high performance NF membranes [11-13]. By alternatively immersing a charged substrate into cationic and anionic polyelectrolytes solutions, a flexibly charged skin layer at nanometer scale is formed, which endows the obtained membranes with desired pure water permeability and satisfied divalent ions rejection. As a facile method in fabricating NF membrane, LBL assembly shows remarkable advantages compared with the conventional interfacial polymerization technique. LBL assembly can precisely control the thickness and composition of the thin films on mono-molecular scale by simply adjusting the deposition parameters. No organic solvents are involved, and therefore, LBL assembly is green and environmentally friendly in general [14]. Moreover, LBL assembly shows great versatility and can be realized by diverse protocols, such as dip/rinse cycles as well as spin and spray processing [15]. Chemical crosslinking process also can be applied to further improve the long-term stability of LBL-based NF membranes [16]. A positively charged hollow fiber NF membrane was designed by our group via inner surface LBL deposition followed by the glutaraldehyde (GA) crosslinking [17]. The obtained NF membrane possessed a thin selectivity layer with superior divalent cation rejection (~90% for Mg^{2+} and Ca^{2+}) and competitive pure water permeability (~17 LMH/bar). More importantly, these results were achieved under the operational pressure of 2 bar, which was lower than the required pressure (> 5 bar) for most commercial NF membranes in the market. Low rejection (< 15%) for Na^{+} ions while maintaining high rejection to divalent ions is the key to obtain such a low operational pressure condition. With these advantages, the feasibility of integrating MBR with this novel low-pressure NF membrane was confirmed by our group as evidenced by a higher removal ability for organic and inorganic foulants compared with the UF-MBR system [18]. Meanwhile, the calculated energy consumption of the NF-MBR + RO system at 90% recovery was comparable to that of UF-MBR + RO at 75% recovery. Nevertheless, the LBL-based low-pressure NF membrane remained vulnerable to fouling when treating MBR effluent. The adsorption of macromolecular organic matters, such as biopolymers, on the inner surface of the NF membrane (with inside-out configuration) could increase the cleaning frequency and maintenance cost. In particular, the structural stability of the LBL deposition layer could be compromised under alkaline conditions [19], in which NaOH solution is commonly used for effective mitigation of protein- or polysaccharides- induced membrane fouling [20, 21]. This in turn limits the application of LBL-based low-pressure NF membrane for water reclamation.

Inspired by the unique adhesion and wettability of mussels in nature, dopamine-based co-deposition provides a promising strategy for constructing antifouling surfaces to overcome the above-mentioned challenges [22, 23]. It has been demonstrated that incorporating low molecular weight polyethylenimine (PEI) into dopamine solutions can promote homogeneous formation of polydopamine (PDA) by suppressing noncovalent interactions within them. This strategy also endows the membrane with uniform and electropositive coating. For example, Chew *et al.* reported the application of PDA/PEI co-deposition in designing antifouling and antiwetting Janus membranes for direct-contact membrane distillation [24, 25]. Meanwhile, the covalent network between PDA and PEI can promote the stability of the selective layer under harsh conditions [26]. Additionally, the non-covalent aggregation of PDA can also be disrupted via interactions with polycations and polyanions, which are necessary components for the LBL layer to further ensure stability of the PDA/PEI co-deposition layer. Combined with the H_2O_2/$CuSO_4$-triggered rapid deposition for PDA/PEI formation to accelerate the co-deposition process without sacrificing operational stability [27], the oxidant-induced PDA/PEI co-deposition provides a new opportunity for tailoring LBL-based low-pressure NF membranes with enhanced fouling resistance and long-term stability. However, very few studies have been reported about the rapid co-deposition of PDA/PEI on LBL layers in preparing antifouling low-pressure NF membranes. And exploring the feasibility of this novel low-pressure NF membrane for MBR integrated with RO system in treating real municipal wastewater for water reclamation was even rare.

In this work, a novel low-pressure NF membrane was designed via electrostatic assembly of LBL layers on PES flat sheet ultrafiltration membrane, followed by PDA/PEI deposition and GA crosslinking. The hierarchical structure and surface chemistry of the newly developed LBL active layer were investigated with a series of characterization methods. Salt rejection and chemical stability were also evaluated by a bench-scale NF apparatus to ascertain its suitability and robustness for long-term filtration process. Moreover, the permeate quality of the NF membrane along with its antifouling ability were examined against real municipal wastewater, followed by testing the fouling potential of NF permeate in subsequent RO membrane. It is hoped that this work could provide new insights into the design of low-pressure NF membranes integrated with

RO unit for water reclamation.

2. Materials and methods

2.1 Materials and chemicals

PES (Ultrason E 6020P, BASF) as a substrate material, polyvinylpyrrolidone (PVP, Alfa Aesar, Mw = 1300 kDa) and anhydrous lithium chloride (LiCl, Merck) as additives, and *N*-Methyl-2-pyrrolidone (NMP, 99%, Merck) as solvent were purchased to fabricate ultrafiltration flat sheet substrate on non-woven support. The non-woven support (novatexx 2484) was obtained from Freudenberg Filtration Technologies SE & Co. KG, Germany. Polyelectrolyte solutions containing sodium chloride (NaCl, Merck) as the supporting electrolyte were prepared with poly (allylamine hydrochloride) (PAH, Mw = 120-200 kDa, Sigma Aldrich) and poly (styrenesulfonic acid) sodium salt (PSS, Mw = 500 kDa, Alfa Aesar). Dopamine hydrochloride, PEI (branched, Mn = 600 Da), tris (hydroxymethyl) aminomethane (Tris, 99.8%), $CuSO_4$ (99%) and H_2O_2 (30 wt.%) were acquired from Sigma Aldrich to prepare the PDA/PEI layer. Glutaraldehyde (GA, 50% in water, Sigma Aldrich) solution was prepared as a crosslinking agent. NaCl, sodium sulfate (Na_2SO_4), magnesium sulfate ($MgSO_4$) and magnesium chloride ($MgCl_2$) (Merck) were used for NF performance tests. The molecular weight cut-off (MWCO) of NF membranes was determined by neutral organic solutes such as glucose, sucrose and raffinose (Merck). Deionized (DI) water was produced by a Milli-Q system (Millipore, USA).

2.2 Development of PDA/PEI modified low-pressure NF membrane

2.2.1 PES substrate preparation and LBL deposition

PES (21.5 wt.%), PVP (0.5 wt.%), and LiCl (3.5 wt.%) were dissolved in NMP in a sealed container at 60 °C and stirred for at least 24 h for complete dissolution. The obtained casting solution was degassed overnight. A casting knife was used to spread the casting solution onto a non-woven support sustained by a clean glass plate at a gate height of 120 μm. Subsequently, the plate was immersed into a coagulant bath containing tap water for phase inversion at room temperature. The nascent PES substrate was kept in DI water for subsequent LBL deposition.

The PES substrate was modified with LBL deposition procedures as reported in previous study

[17]. In brief, the freshly prepared PSS solution (50 mL, 4 g/L with 30 g/L NaCl, original pH) was first poured into a customized membrane holder (effective modification area of 72 cm^2) where only the active layer of the PES substrate was exposed to the polyanion solution for 15 min. After rinsing with DI water, the surface of anionic polyelectrolyte-loaded substrate was contacted with PAH solution (50 mL, 10 g/L with 150 g/L NaCl at a pH 2.3) for 10 min, followed by another DI water rinsing. The multiple PSS/PAH bilayers were prepared by repeating the steps described above (10 min for each deposition). In the current work, NF membrane with 2.5 PSS/PAH bilayers were fabricated, which was denoted as LBL. For the crosslinking process, the GA solution (50 mL, 0.1 wt.%) was contacted with the surface of the LBL membrane for 15 min. After rising with DI water, the crosslinked LBL membrane (referred as cLBL) was immersed in DI water for further characterization and evaluation.

2.2.2 Co-deposition of PDA/PEI triggered by $CuSO_4/H_2O_2$

The PDA/PEI modification was performed on the surface of LBL-based membrane based on an improved method [27]. Dopamine (2 mg/mL), PEI (2 mg/mL), and $CuSO_4$ (8.3 mM) were first dissolved in Tris buffer solution (50 mL, pH 8.5, 50 mM), followed by the addition of H_2O_2 (32.6 mM) into the mixed solution to prepare the deposition solution. Then, the freshly prepared solution was poured into the previously mentioned membrane holder where only the LBL layer of the NF membrane contacted the solution for designated times (0.5 – 4 h) at room temperature. After modification, the membrane was rinsed with DI water several times. The optimized membrane was labelled as LBL-PP with modification time of 2 h. Subsequently, LBL-PP membrane was crosslinked with GA solution for 15 min. We termed this membrane as LBL-cPP. The samples were then rinsed and submerged in DI water overnight for later use. A scheme for the fabrication procedures and designations of various membranes, *i.e.* membrane ID, is provided in Fig. A1 for easy reference.

2.3 Membrane characterization

2.3.1 Characterizations of membrane morphologies and properties

The deposition density (DD, mg/cm^2) of LBL-cPP membrane was measured by the weight method with previously reported procedures [28]. The measured membranes area was 20 cm^2.

Each result was the average of at least five parallel measurements on different membrane samples. Before the measurements, the ultrasonic treatment of membranes was conducted for at least 10 min in an ultrasonic bath (FB 15068, Fisher Scientific, USA).

The morphologies of the PES substrate and prepared NF membranes were observed by a field emission scanning electron microscope (FESEM, JSM-7600F JOEL, Japan) at 5 kV. Their cross-sectional structures were further characterized with a JEM 1400 transmission electron microscope (TEM) at 80 kV. The preparation procedure of membrane samples for TEM observation was according to previous work [29]. The topologies and roughness of the membranes were examined through an atomic force microscope (AFM, XE-100, Park Systems, Korea) operated under non-contact mode. The chemical composition of membrane surface was surveyed by an X-ray photoelectron spectroscopy (XPS, AXIS Supra, Kratos Analytical, UK) with a monochromatic Al Kα excitation source and analyzed by CasaXPS software. A Fourier transform infrared spectroscope with attenuated total reflectance mode (ATR-FTIR, IR-Prestige-21, Shimadzu, Japan) was also used to analyze the functional groups on the membrane surface. The water contact angles of NF membranes were elucidated with a goniometer (Contact Angle System OCA, Data Physics Instruments GmbH, Singapore). The charge property of the membrane surface was detected using a streaming potential method by an electro-kinetic analyzer (SurPASS^{TM} 3, Anton Paar, Austria) with 1 mM NaCl solution as electrolyte solution.

2.3.2 NF performance evaluation

The performances of the designed NF membranes and commercial flat sheet NF membrane (FILMTEC^{TM} NF 270 from Dow Chemical) were measured by a bench-scale crossflow filtration unit with an effective membrane area of 40 cm^2. Each membrane coupon was housed in a membrane cell (schemed in Fig. A2) while ensuring that the pure water/salt solutions always faced the membrane active layer. The pure water permeability, salt water permeability (expressed in unit of $L/m^2h \cdot bar$ abbreviated as LMH/bar) and salt rejection of NF membranes were determined at 2 bar pressure with a crossflow velocity of 0.3 m/s (laminar). The single salt rejection evaluation (repeated with five different samples for each type of membrane) was conducted with NaCl, $MgCl_2$, Na_2SO_4, and $MgSO_4$ solutions at a concentration of 1000 ppm, based on the conductivity

measurement (Ultrameter II, Myron L Company, Canada) of the feed and permeate solutions. A series of neutral organic solutes such as glucose, sucrose and raffinose were used to detect the MWCO of the membranes following the same testing protocols [17].

Moreover, the chemical stability of designed membranes was evaluated according to variations in NF performance during a long-term operation process with pure water and chemical solutions such as hydrochloric acid solution (HCl, pH 3) and sodium hydroxide solution (NaOH, pH 10). In detail, the as-prepared membranes were continuously tested on the apparatus for 50 h with pure water and then the $MgCl_2$ rejection was measured. For the stability evaluation under acidic/alkaline condition, the HCl/NaOH solution was filtrated across the membrane surface without pressure for 1 h followed by DI water cleaning and the evaluations of pure water permeability and $MgCl_2$ rejection. Three different samples for each type of membrane were used for stability evaluation.

2.4 NF performance using municipal wastewater

In order to explore the antifouling and separation properties of low-pressure NF membranes in real applications, a systematic study was carried out against municipal wastewater collected from a wastewater treatment plant in Singapore (sieved with a 1 mm opening mesh). The municipal wastewater was filtrated through a 0.45 μm microfiltration membrane (AP series, KAREI^{TM} FILTRATION) prior to use as the feed solution for the NF process. The total organic carbon (TOC), salt concentrations and conductivity of feed solution are given in Table 1.

Table 1. Water quality of the feed solution for NF process.

Parameter	Value
TOC (mg/L)	23.4 ± 2.6
Ca^{2+} (mg/L)	22.6 ± 3.1
Mg^{2+}(mg/L)	4.6 ± 1.2
Na^{+}(mg/L)	73.3 ± 4.2
Conductivity (μs/cm)	835.4 ± 15.1

pH	6.9 ± 0.2

In this study, the cLBL, LBL-cPP and commercial flat sheet NF 270 membrane were selected to evaluate their antifouling and separation performances. The pre-treated municipal wastewater was added to the feed tank with an effective volume of 5.0 L and pumped to the mentioned membrane filtration cell at 2 bar. The NF retentate and NF permeate were recirculated to the feed tank, and the test solution in the feed tank was replenished daily. Periodic physical membrane cleaning of 30 min flushing with DI water at 500 mL/min was performed when the flux drop reached the pre-set limit due to membrane fouling. Total of three consecutive fouling-cleaning cycles were performed for each membrane. Only one sample of each type of NF membrane was applied for treating wastewater at the same crossflow conditions mentioned in Section 2.3.2. The pressures of feed and permeate along with the permeate flow were recorded by the previous measuring apparatus and logging system [18].

A RO system was employed to investigate the fouling potentials of the respective permeates from the NF 270, cLBL and LBL-cPP NF membranes. The permeates were collected from the separated NF filtration setup with pre-treated municipal wastewater mentioned above. The details of the RO system and test protocol had previously been described [30]. The crossflow velocity was maintained at 0.10 m/s.

2.5 Analytical measurements

The adhesion forces (F/R) between foulant and membrane were detected by the AFM under contact mode with a commercial V-shaped SiN probe (spring constant of 0.06 N/m, Novascan Technologies, Inc., USA) which was modified with a 5.0 μm PEG-NH_3 coated SiO_2 particle on the end of the cantilever. Before the measurement, the probe was coated with foulants. The detailed foulants coating process and adhesion force measurement were in accordance with the reported procedure [31].

The concentrations of Ca^{2+}, Mg^{2+}, and Na^{+} ions in the feed and permeate solutions of the NF process were determined by an inductively coupled plasma optical emission spectrometry (ICP-

OES, Optima 8000, Perkin Elmer, USA). TOC was detected by a TOC/TN-V analyzer (Shimadzu, Japan). An excitation emission matrix (EEM) fluorescence spectra of feed, permeate and foulants on the NF membrane surface were obtained by a LS 55 fluorescence spectrometer (Perkin Elmer Company, USA). The dissolved organic fractions in the samples were also characterized by a liquid chromatography-organic carbon detection (LC-OCD, Model 8, DOC-LABOR, Germany). The foulants were extracted from the membrane surfaces by immersing the membranes into 25 ml of DI water and ultrasonication for 30 min, followed by 1 min vortex.

3. Results and discussion

3.1 Surface structures of the membranes

A series of factors, such as dopamine concentration, deposition temperature, deposition time, and oxidant types, influenced on the deposition process of PDA on membrane surface [32]. Based on previous work [27], the dopamine concentration of 2 mg/mL and deposition temperature at 25 ^{o}C have been confirmed as the optimal conditions for controlled PDA/PEI deposition under the trigger of $CuSO_4/H_2O_2$ (oxidants). In this work, in order to explore the effect of the LBL layer on the PDA/PEI deposition process, the deposition times of PDA/PEI were investigated as shown in Fig. 1. With extending the deposition time, the deposition density gradually increased and remained steady at 0.378 ± 0.017 mg/cm^2 after 2 h. It could be attributed to the precipitation of the PDA aggregates from the deposition solution, which in turn could hardly be deposited on the LBL layer. Therefore, 2 h was selected to be the optimal coating time for PDA/PEI on the LBL layer. This result was slightly different from previous report, which indicated the completion of PDA/PEI coating within 1 h on hydrolyzed polyacrylonitrile membrane [27]. This phenomenon could be rationalized by the size control-inhibition mechanism of PDA in the presence of polycations and polyanions [26]. Unprotonated amino groups of PAH (polycation) in the LBL layer could bind covalently to quinone groups of PDA by competing with amino groups of Tris buffer [33, 34], which caused the size decrease of PDA aggregates. Besides, PSS (polyanions) could further suppress the PDA deposition [34]. Therefore, the co-deposition process of PDA/PEI on the LBL layer was delayed, even though the rapid deposition was induced using $CuSO_4/H_2O_2$ as a trigger.

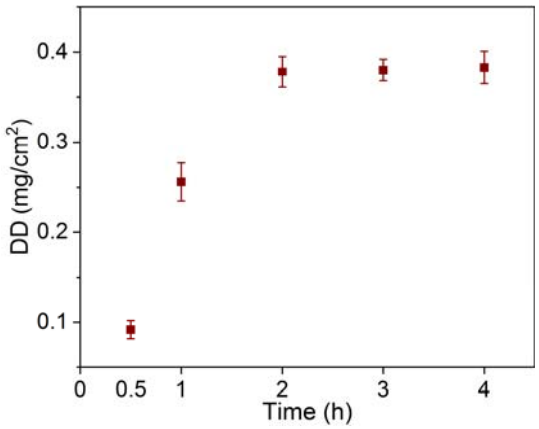

Fig. 1. Time-dependence of deposition density (DD) for the PDA/PEI coatings at 25 ºC.

ATR-FTIR and XPS measurements were used to elucidate the surface chemical structures/compositions of the designed membranes. As presented in Fig. 2, a new peak that was absent on the PES substrate emerged at 1036 cm^{-1} on the modified membrane surfaces. This was attributed to the symmetric vibration of the $-SO_3$ group in PSS, indicating the successful deposition of the LBL layer [35]. As a result of the co-deposition of PDA/PEI, the intensity of peak around 3000−3650 cm^{-1} ascribing to −OH and −NH stretching was enhanced. This demonstrates the presence of catecholamine in the PDA structure [36] and 2º-amines in the PDA/PEI co-deposition layer [37]. Fig. 2(B) shows the XPS survey spectra of different membranes and their corresponding elemental compositions are listed in Table 2. Compared with the LBL and cLBL NF membranes, a more intense N 1s peak was observed in the spectrum of PDA/PEI modified LBL NF membranes. The atomic percentage of N increased from 3.63% to 9.32% after the deposition of PDA/PEI. This increase was a result of the high percentages of nitrogen in both PDA and PEI structures. The atomic ratio of O/N (1.84) in the LBL-PP membrane was similar to the theoretical O/N value (2.00) for pure dopamine monomer [38], indicating that the PDA/PEI layer well covered the LBL-based membrane. This was further confirmed by the disappearance of Na 1s and S 1s peaks in the wide spectra of the LBL-PP and LBL-cPP membranes in Fig. 2(B). It should be noted that the S element (existed in $-SO_3$ group of PSS) could still be detected with ATR-FTIR after the deposition of PDA/PEI due to the deeper analysis depth of the ATR-FTIR as compared to the XPS.

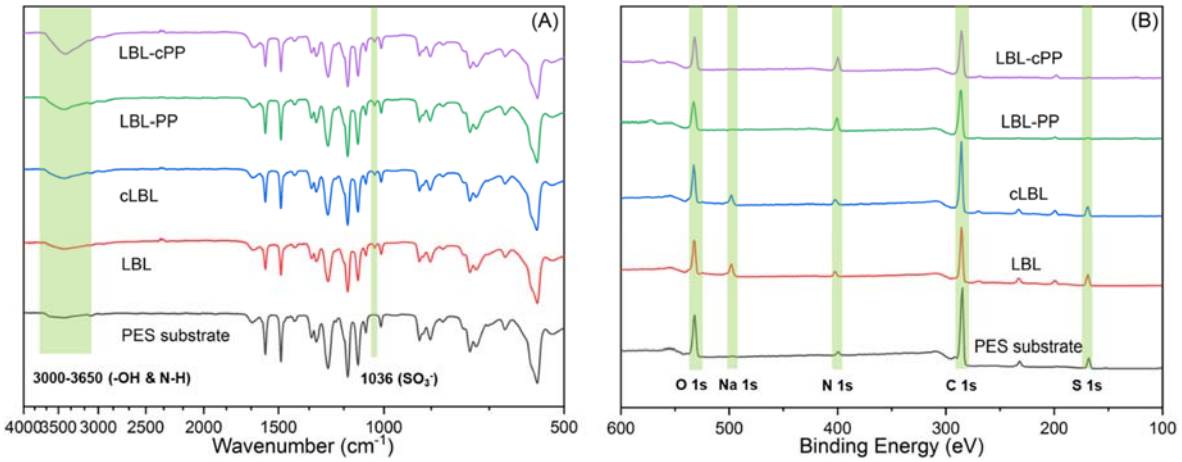

Fig. 2. (A) ATR-FTIR and (B) XPS spectra of different membranes.

Table 2. Element composition for PES substrate and developed NF membranes.

Membrane	C (%)	N (%)	O (%)	S (%)	Na (%)	Cu (%)	O/N
PES substrate	75.26	1.69	17.49	5.56	–	–	10.3
LBL	70.49	3.63	15.74	8.04	2.10	–	4.34
cLBL	72.15	3.63	15.24	7.77	1.21	–	4.20
LBL-PP	72.57	9.32	17.19	0.53	–	0.39	1.84
LBL-cPP	71.55	9.90	17.75	0.42	–	0.38	1.79

The possible chemical bonding in the membrane surface was further explored with high-resolution XPS C 1s of the PES substrate and NF membranes (Fig. 3(A-D)). The intensity of C 1s component peak at 286 eV (C-O/C-N) for cLBL membrane was slightly stronger than that for the PES substrate. This demonstrated that more C-N bonding was formed by crosslinking between amino groups of PAH and aldehyde groups of GA. With the PDA/PEI coating on the LBL layer, the intensity of C-N peak was further enhanced (Fig. 3(C)). This observation could be rationalized from a phenol-amine based covalent bond formation via Michael addition between PDA and PEI [23]. A new C 1s component peak also emerged at 288.5 eV (C=O), which was attributed to the presence of quinone groups in PDA structure. The intensity of C-N peak was obviously higher for the LBL-cPP membrane as consistently observed by the ATR-FTIR result. This could be explained by the abundant amine groups in PDA/PEI that induced sufficient crosslinking reaction. Besides, the crosslinking between the LBL layer and PDA/PEI by GA might also be triggered. These results all confirm the well deposition of a PDA/PEI layer and its enhanced interconnection with LBL

layer. It should be noted that dopamine quinone was formed during the polymerization of dopamine [27], which reduced the density of the benzene groups on the PDA/PEI layer. Therefore, the signal of π-π* stacking was hardly detected by the XPS (Fig. 3 (C-D)).

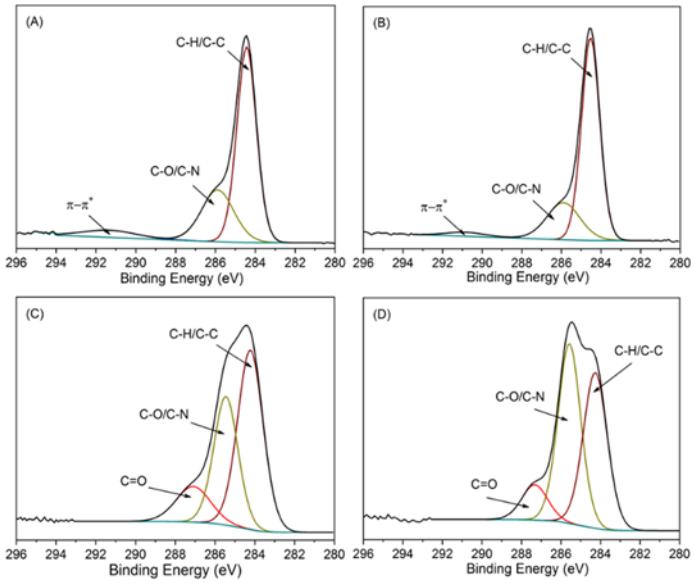

Fig. 3. High-resolution spectra of C1s for (A) PES substrate, (B) cLBL, (C) LBL-PP, and (D) LBL-cPP membranes.

3.2 Morphologies and surface properties of the membranes

The FESEM images (Fig. 4(A-F)) show surface and cross-sectional morphologies of the PES substrate, cLBL and LBL-cPP membranes. The PES substrate presented a smooth and porous surface morphology, while a rough and compact surface with irregular topography was observed for the cLBL membrane (Fig. 4(B)). This characterization once again confirms a full coverage of polyelectrolyte depositions on the substrate. This result was vindicated by AFM images that presented increased roughness (R_a) from 2.22 ± 0.78 nm for the PES substrate to 12.62 ± 0.91 nm for the cLBL membrane (Fig. A3). After the introduction of a crosslinked PDA/PEI layer, a rougher surface with grainy and convex nanostructures was observed for the LBL-cPP membrane (Fig. 4 (C) and Fig. A3(D)). This indicated fewer visible PDA aggregates were deposited on the LBL layer. This phenomenon could be attributed to the diminishing of non-covalent interactions in the PDA aggregates caused by nucleophilic amine groups of the PEI molecules [27]. Meanwhile, the aggregation of PDA was also disrupted by the size control-inhibition mechanism of polyelectrolytes as discussed above. Eventually, the PDA/PEI deposition layer tailored the NF

membrane with a homogeneous surface. By referencing to the FESEM images, the thickness of the PES substrate and cLBL membrane were compared. After PDA/PEI deposition, the average thickness of the crosslinked PDA/PEI coated LBL layer was increased to 116.1 ± 5.2 nm (Fig. 4 (F)), compared with the single crosslinked LBL layer (thickness of 48.8 ± 5.0 nm in Fig. 4 (E)). The corresponding TEM images (Fig. 4 (G-I)) also confirmed the thickness variations of the coated layers, which revealed that the PDA/PEI deposition layer was uniformly and compactly anchored on the LBL surface. More importantly, the PDA particles could be observed in the deposition layer (Fig. 4 (I)), further demonstrating effective inhibition of PDA aggregation.

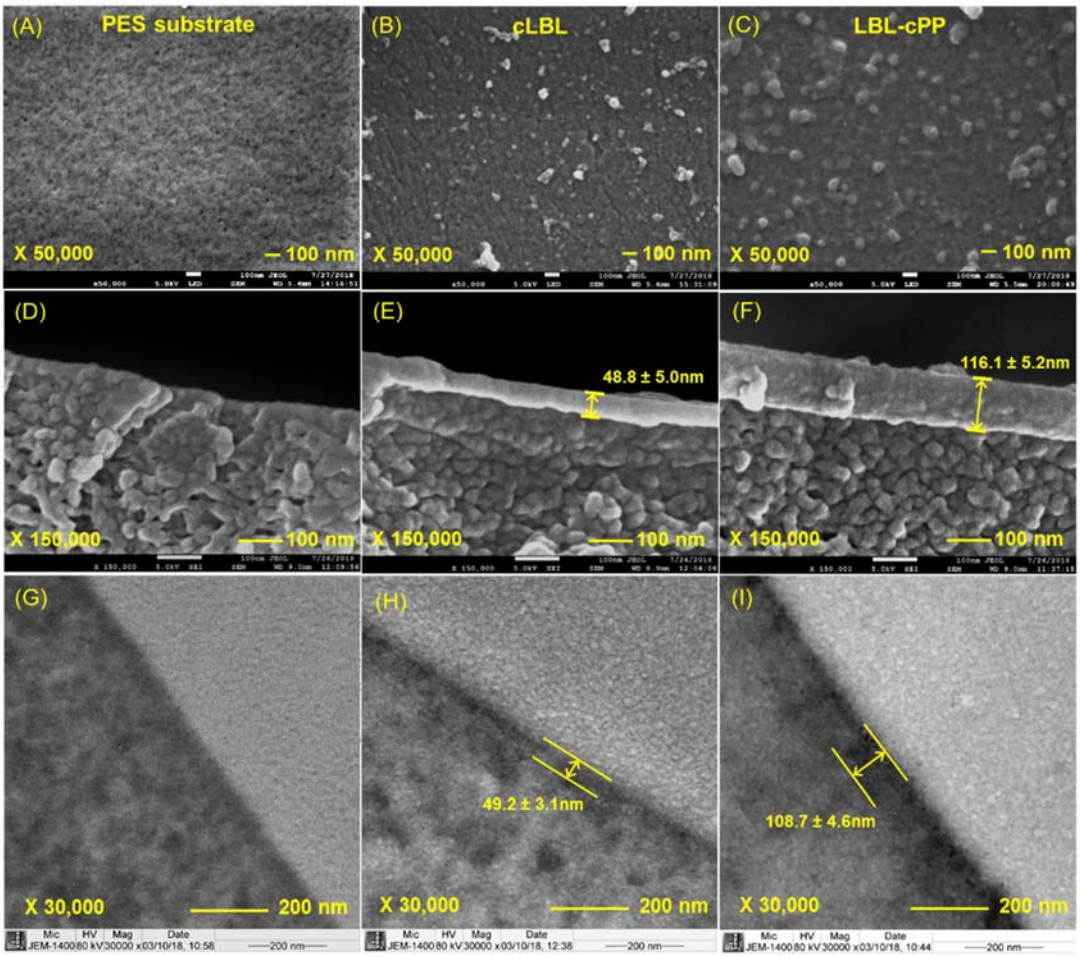

Fig. 4. FESEM images of surfaces (A-C) and cross-sections (D-F), and TEM images of cross-sections (G-I) of PES substrate (A, D, G), cLBL (B, E, H), and LBL-cPP (C, F, I) membranes.

As more amine groups were introduced onto the surface by PDA/PEI co-deposition, the surface hydrophilicity and charge property of the respective membranes were altered. As depicted in Fig. 5(A), the contact angle of the PES substrate was 80.0° and exhibited few signs of sliding

with time, indicating its strong hydrophobicity. With the crosslinked LBL deposition layer, the surface contact angle was measured at 40.0° and gradually decreased to 18.3° as time increased to 600 s. This could be attributed to the hydrophilic nature of the PSS ($-SO_3$) and PAH ($-NH_3$) structures. After the PDA/PEI modification, the contact angle further declined to about 20.0° and the water droplet eventually spread across the membrane within 200 s, suggesting an excellent wettability. This performance may significantly extend the prospect of the LBL-cPP NF membrane in antifouling application. Fig. 5(B) presents the zeta potential versus pH curves of the PES substrate and designed NF membranes. The PES substrate possessed a negatively charged surface with an isoelectric point of pH = 4.0, which was similar with reported data [17]. After the binding of PDA/PEI co-deposition layer, the zeta potential curve of the LBL-PP membrane shifted to the basic region significantly and the isoelectric point increased to pH = 7.2. It should be noted that the positive charge was reduced slightly after crosslinking for the LBL-cPP membrane probably due to the depletion of amino groups by reacting with aldehyde groups in GA. Nevertheless, the LBL-cPP membrane was still positively charged in general pH range of wastewater treatment process, which would be beneficial in rejecting divalent cations.

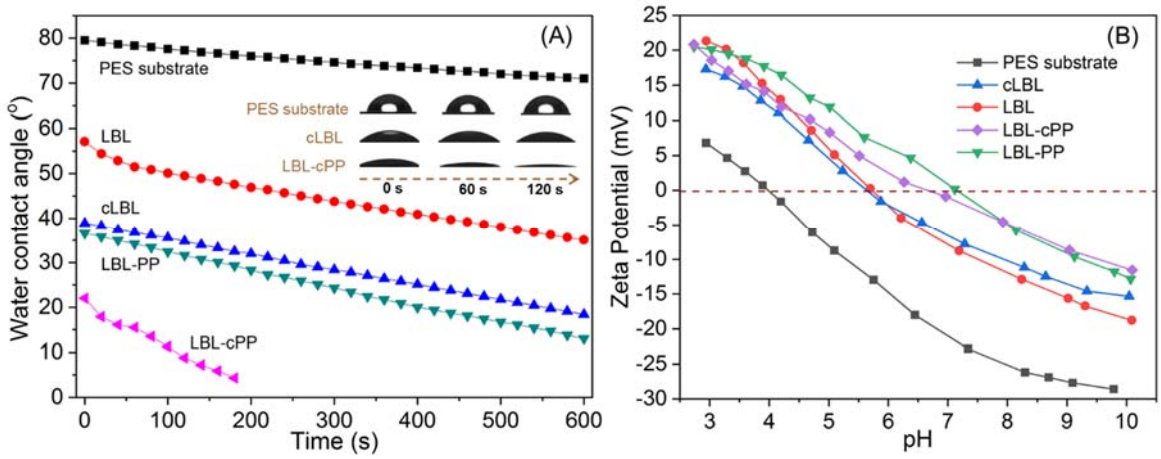

Fig. 5. (A) Water contact angle of the water droplet with increasing time on different membranes surfaces; (B) zeta potential as a function of pH of different membranes.

3.3 Nanofiltration performance

The MWCO of the respective membranes was estimated by testing the neutral solute rejection. Upon the crosslinking process, the pore size of the membrane surface was reduced with higher rejections against all tested neutral solutes. As listed in Table 3, the MWCO values of the

LBL and cLBL membranes were around 500 Da and 465 Da, respectively, by plotting their rejections against solute molecular weights. With the coating of PDA/PEI on the LBL layer, the selective layer of the LBL-PP membrane became even tighter with a MWCO of 419 Da. As previously mentioned, PEI destroyed the non-covalent bonds within PDA aggregates to render the PDA/PEI co-deposition layer uniform. Meanwhile, the polyanions in LBL layer could form a crosslinked network with PDA through covalent bonds although both polycations and polyanions could interrupt the non-covalent aggregation of PDA. Therefore, a dense PDA/PEI layer with reduced pore size was formed on the LBL layer. Moreover, the MWCO of the LBL-cPP membrane was further reduced to 361 Da when GA crosslinking was conducted on the surface, which was attributed to the existence of abundant amine groups in the PDA and PEI structures.

Table 3. Rejection performance of neutral solutes [a]

Neutral solute	NF 270	LBL	cLBL	LBL-PP	LBL-cPP
Glucose [b]	53.5%	57.8%	59.9%	64.6%	72.1%
Sucrose [c]	80.2%	83.0%	85.2%	86.6%	89.1%
Raffinose [d]	87.9%	90.2%	91.5%	93.8%	96.8%

[a] concentration: 200 ppm, operating pressure: 1 bar, crossflow velocity: 0.3 m/s (laminar);
[b] M_W = 180 Da, r_s = 0.36 nm;
[c] M_W = 342 Da, r_s = 0.46 nm;
[d] M_W = 504 Da, r_s = 0.54 nm.

The designed membranes were further characterized with a typical NF process. Fig. 6 portrays the permeability and rejection of NF membranes against various inorganic salts at 2 bar using NaCl, Na_2SO_4, $MgSO_4$ and $MgCl_2$ solutions as feed solutions, respectively. As depicted in Fig. 6(A), a drastic decrease in pure water permeability from 110.0 LHM/bar for PES substrate to 13.1 LHM/bar for the cLBL NF membrane was observed. This drop further mirrored the strong and effective coverage of polyelectrolytes on the substrate surface. Both pure water and salt solution permeability further decreased with the co-deposition of crosslinked PDA/PEI layer on the LBL membrane, despite its hydrophilic nature. As discussed in Section 3.2, the coating of PDA/PEI increased the thickness of selective layer, thereby enhancing the hydraulic resistance through the membrane to both water and salt. In addition, the dual covalent reactions of PDA with

PEI and polyelectrolytes in the LBL layer tightened the selective layer structure of the NF membrane, which induced decreased permeability. On a different note, the pure water permeability can be further improved by reducing the thickness of the substrate, increasing the ionic strength (NaCl concentration) of the polyelectrolyte solution, reducing the number of LBL layers, and controlling the crosslinking reaction. A systematic investigation of these parameters will be a focus in our future studies. Despite this, an obvious elevation in all salt rejections was witnessed for the PDA/PEI modified LBL membrane as compared to the LBL membrane (Fig. 6 (B) and Table A1). Particularly, the PDA/PEI coating conferred a fairly high Na_2SO_4 rejection to the LBL membrane; the rejection improved from 37.4% to 57.8% (Table A1). Such a higher rejection generally benefits from the size exclusion enabled by a denser selectivity layer. Nevertheless, this improvement comes at the sacrifice of pure water permeability. In the case of the commercial NF 270 membrane, the 'loose' and negatively charged nature was revealed as an evidence by the higher rejection against Na_2SO_4 and lower rejection for $MgCl_2$ (Fig. 6(B)). As already been attested by previously study, such an observation suggested that the Donnan exclusion theory played a major role [17]. On the other hand, the salt rejection test suggested that the LBL-cPP NF membrane reached the 90% rejection for divalent cations and about 20% rejection for monovalent cations, while maintaining the order of $MgCl_2$ > $MgSO_4$ > Na_2SO_4 > NaCl. This result was reasonable for positively charged NF membrane and corroborated the benefits of a relatively dense selectivity layer brought about by the co-deposition of PDA/PEI. Therefore, it can be concluded that similar results on $MgSO_4$ rejection between the NF 270 and LBL-cPP membranes were due to different dominant rejection mechanisms.

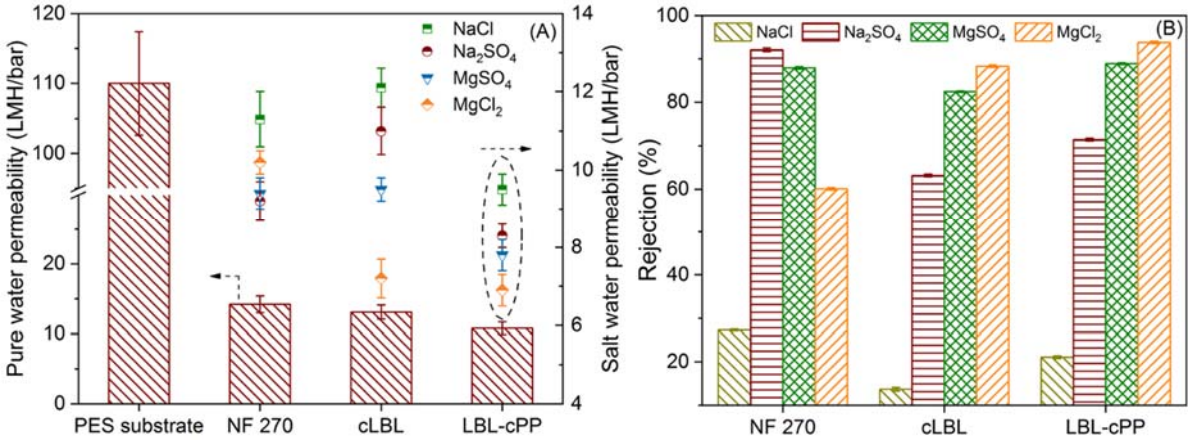

Fig. 6. Permeability (A) and separation (B) performance of PES substrate, NF 270 and designed

NF membranes (Experimental conditions: salt concentration, 1000 ppm; crossflow velocity, 0.3 m/s; pH 6; operating pressure, 2 bar; temperature, 25 ± 0.5 °C).

Comparing with the current NF performances of LBL-based NF membranes from literature, the LBL-cPP flat sheet membrane fabricated in this work exhibited competitive performance on salt permeability and rejection under a relatively low operating pressure as shown in Table 4. It could be explained by the hydrophilic nature of PDA/PEI co-deposition layer and the dual covalent reactions of PDA with PEI and LBL components that tightened the selective layer of the designed NF membrane. These combined advantages could render the NF membrane effective organic fouling control and superior separation performance in real wastewater treatment process, as discussed in the following Section 3.5.

Table 4. Comparison of salt permeability and rejection of various LBL-based NF membranes.

Membrane	$MgCl_2$		$MgSO_4$		Testing conditions		References
	Permeability (LMH/bar)	Rejection (%)	Permeability (LMH/bar)	Rejection (%)	Salt concentration (ppm)	Operation pressure (bar)	
LBL-cPP	6.9	93.8	7.8	88.9	1000	2	**This work**
LBL flat sheet	4.0	93	–	–	4000	4.8	[39] 2008
((PEI-modified GO)/PAA)$_1$/PVA/GA	–	–	1.24	84.1	1000	5	[40] 2012
(PDDA/GO)$_4$	–	–	6.95	69.2	1000	5	[41] 2016
(PEI/GO/PEI)/h	4.2	93.9	4.2	80.0	100	6.2	[42] 2016
GO LBL	–	–	–	63	1000	3	[43] 2016
Graft PDA/PEI/SiO_2	5.5	89	4.7	70	1000	6	[44] 2017
BPPO/EDA/GO	–	–	–	46	1000	1	[45] 2018
Crosslinked (CS/PAA)$_4$	~1.11	~31	~0.93	~93	500	7	[46] 2018

3.4 Performance stability of LBL-cPP NF membrane

The chemical stability of membrane plays a crucial role in practical applications due to the

need for regular chemical cleaning. The covalent polymerization and non-covalent self-assembly synergistically induce the formation of PDA coatings [47], whereas the non-covalent parts are unstable under harsh conditions [48]. It is well known that the increase of crosslinked structure in coating layer by oxidization will enhance the coating stability [49]. $CuSO_4/H_2O_2$-triggered PDA/PEI co-deposition process creates more covalent parts and crosslinked sites that will be further strengthened by the interactions with the LBL layer to improve coating stability. In this study, the stability of the cLBL and LBL-cPP NF membranes was tested under different treatment conditions. All the membranes showed a stable permeability and $MgCl_2$ rejection after continuous operation of 50 h with DI water (Fig. A4(A)). Similarly, the permeability and $MgCl_2$ rejection of the cLBL and LBL-cPP membranes experienced little change after the treatment of an acidic solution at pH 4 (Fig. A4(B)), indicating good performance stability under acidic environment. However, a remarkable increase for permeability was observed for the cLBL membrane after alkaline treatment (Fig. 7). This demonstrated that the LBL layer was irreversibly swelled due to deionization of amine groups on the PAH polymer chains under strong alkaline condition [19]. Accordingly, the $MgCl_2$ rejection of treated the cLBL membrane dropped by 20% after three alkaline treatment cycles. In contrast, the rejection loss was negligible for the LBL-cPP membrane, which was due to the covalent crosslinking of PDA/PEI on the LBL layer. These results signify that the PDA/PEI coating on the LBL layer exhibited outstanding stability and durability, demonstrating its great potential in practical chemical cleaning.

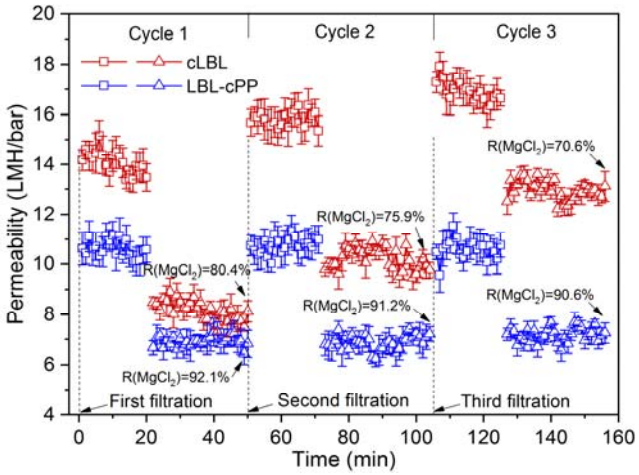

Fig. 7. Alkaline stability test of NF membranes (Test procedure and conditions for each cycle: alkaline treatment (1h without pressure) -> pure water permeability test (20 h, 2 bar, presented as squares) -> $MgCl_2$ rejection test (30 h, 2 bar, presented as triangles)). The original permeability

and $MgCl_2$ rejection for cLBL and LBL-cPP membranes were 13.1 LMH/bar, 88.3 % and 10.8 LMH/bar, 93.8 %, respectively.

3.5 Membrane performance using municipal wastewater

3.5.1 Flux profiles of NF membranes

The flux profiles of the NF 270, cLBL and LBL-cPP membranes under continuous filtration mode with real municipal wastewater are illustrated in Fig. 8. The decline in permeability was observed for all NF membranes, which could be attributed to the 1) deposition of predominantly rejected inorganic ions and organic molecules on the membrane surface and the 2) formation of cake/biofilm layer originated from the build-up of colloidal particles, soluble microbial products and microorganisms. The periodical cleaning of NF membranes was performed when the permeability dropped to 80% of the initial flux. As seen in Fig. 8, the flux of NF 270 dropped almost linearly from the starting point and required the most frequent cleaning among all membranes. In addition, the flux was not able to recover after each cleaning process indicating irreversible fouling on the membrane surface. For the cLBL membrane, the interval between each cleaning cycle was extended, indicating lower fouling rate and better antifouling ability. As mentioned above, LBL deposition ameliorated the hydrophilicity of the resultant NF membrane, which effectively maximized the surface hydration and alleviated the foulants adsorption. Hence, the membrane was more easily recovered after regular physical cleaning.

It is interesting to note that the PDA/PEI layer further improved the antifouling performance of the NF membrane. As illustrated in Fig. 8, the water flux of the LBL-cPP membrane dropped slightly from an initial value of 10.2 LMH/bar within 10 h after commencement and maintained around 9.7 LMH/bar for 50 h during the stabilization period. Overall, only 7.4% loss in flux was noticed after 60 h of filtration, thus no physical cleaning was required. The ameliorated antifouling performance for the LBL-cPP membrane might be derived mainly from the desired hydrophilicity that had been confirmed by contact angle measurements in Fig. 5 (A). The adhered foulants on the LBL-cPP membrane surface could be more readily removed by shear force than those on the cLBL and NF 270 membranes. This could result in less irreversible fouling. Moreover, the lower MWCO of LBL-cPP membrane may suffer from less pore blocking and pore plugging, which was

considered as the main reason for the irreversible fouling. Therefore, it exhibited better fouling resistance and lower cleaning frequency as compared to the cLBL and NF 270 NF membranes. More systematic fouling experiments including flux stepping, irreversible fouling *etc.* will be carried out in our future study. Despite this, the flux of LBL-cPP membrane may not be fully retrieved by periodical cleaning. It could be attributed to its slightly higher surface roughness and positively charged surface.

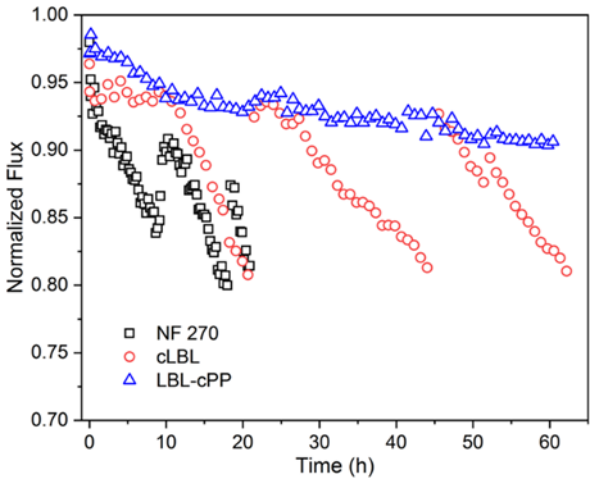

Fig. 8. Flux profiles of NF 270, cLBL and LBL-cPP membranes filtrated with municipal wastewater (Membrane was cleaned when the normalized flux was 0.8. LBL-cPP was not cleaned). The initial permeability for NF 270, cLBL and LBL-cPP membranes were 13.9, 13.0 and 10.2 LMH/bar, respectively.

The foulant–membrane interaction forces were characterized with AFM force measurements for better exploring the surface property responsible for fouling behaviors of different NF membranes. The interaction between AFM probe and membrane surface broke easily when the probe pulled off from the membrane surface, which caused similar curve trends for the NF 270, cLBL and LBL-cPP membranes (Fig. 9 (A)). However, the maximum adhesion force for the LBL-cPP membrane was lower than that for the NF 270 and cLBL membranes, indicating lower attractive energy for retracting the probe from the membrane surface. This provides clear evidence confirming the enhanced antifouling property with PDA/PEI coating on the LBL layer. The corresponding frequency distribution is presented in Fig. 9(B). The adhesion force distribution for NF 270 moved to more negative values, indicating larger adhesion forces comparing to the newly developed NF membranes, which was in accordance with the trend of adhesion force curves. By

contrast, the foulant-membrane adhesion forces of the LBL-cPP membrane were distributed within a narrow range (from -1.20 to -0.13 mN/m) and centered at low adhesion forces values (average force of -0.59 mN/m), which could be explained by the weakened adhesion force between the LBL-cPP membrane surface and foulant molecules induced by its enhanced surface hydrophilicity. Considering the flux profiles of the NF 270, cLBL and LBL-cPP membranes with municipal wastewater (Fig. 8), it is clear that the stronger the adhesion force of the foulant-membrane, the more obvious the flux decline is. The PDA/PEI layer impaired the adsorption of organic foulants on NF membrane surface, reducing the cleaning frequency and extending its service lifespan in real separation against municipal wastewater. This confirms the potential application of our developed membrane in water reclamation.

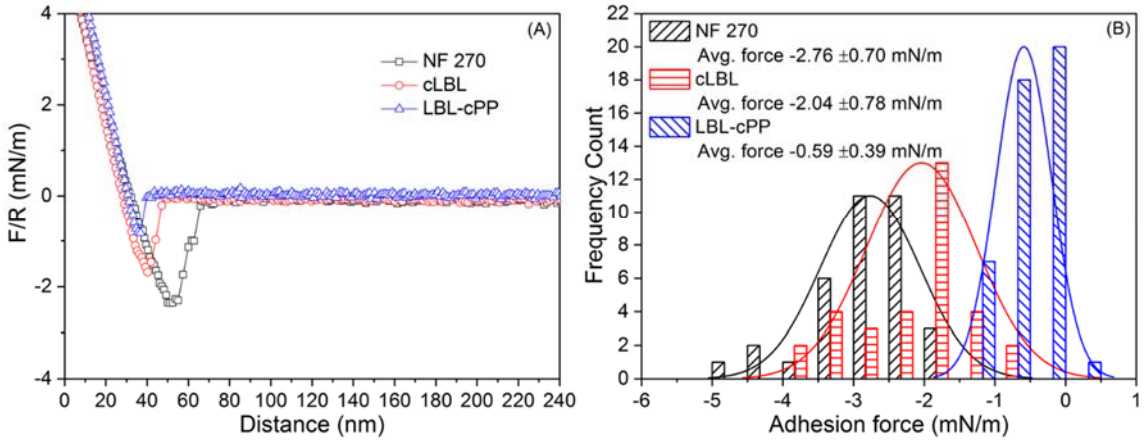

Fig. 9. (A) Representative adhesion forces and (B) frequency distribution of foulant-membrane adhesion forces for NF 270, cLBL, and LBL-cPP membranes.

3.5.2 Organic compositions

The practical recovery of RO process is confined by fouling, such as inorganic scaling, organic fouling and biofouling [50]. In water reclamation processes, elevating the feed water quality for RO process has been considered as the effective approach to control RO fouling. As shown in Table 5, the permeate qualities of the NF 270, cLBL and LBL-cPP membranes were evaluated. Due to superior rejection of the LBL-cPP membrane, the permeate of LBL-cPP presented lower TOC (~90.6% lower), Ca^{2+} (~76.9% lower), Mg^{2+} (~95.6% lower) and Na^{+} (~40.4% lower) as compared to the feed solution, which was better than that of NF 270 and cLBL processes. The EEM fluorescence spectra provide better understanding of the organic

compositions in the permeate for each process as well as its surface foulants. As depicted in Fig. 10 (A), the EEM plots for feed solution were classified into four sections - I (humic-like substances; Ex > 280 nm, Em > 380 nm), II (protein-like substances; Ex = 250−280 nm, Em < 380 nm), III (fulvic acid-like substances; Ex = 220−250 nm, Em > 380 nm), and IV (tyrosine-like substances; Ex = 220−250 nm, Em = 330−380 nm) [51]. A distinct peak for tyrosine-like substances (IV) could be observed in feed solution, which are typically proteinaceous and associated with amino acids. After the filtrations, the peak intensities of tyrosine-like substances (IV) decreased by 84.2%, 89.3% and 93.9% for the permeates of the NF 270, cLBL and LBL-cPP membranes, respectively, compared to the feed solution, indicating better removal efficiency for tyrosine-like substances. In particular, the LBL-cPP membrane presented significant removal efficiency (decreased by 96.1%) for protein-like substances (II) from the feed solution, which was confirmed by its almost disappearing peak intensity (Fig. 10 (A)). Hence, the LBL-cPP membrane has a higher capacity to provide better permeate quality. It should be noted a small amount of fulvic acid-like substances (III) were identified in the permeate of all NF membranes. This is most likely due to their smaller molecular weights than the MWCOs of the NF membranes. Meanwhile, simpler organic compositions were illustrated by the foulant on the surface of the LBL-cPP membrane, which were composed of very small amounts of protein-like substances (II) and part of tyrosine-like substances (IV) that appeared far less than the amount on NF270 and cLBL (Fig. A5). These results were consistent with the flux profile of the LBL-cPP membrane. Owing to the competitive hydrophilicity of the LBL-cPP membrane, most of the humic-like substances (I) and protein-like substances (II) did not adsorb onto the membrane surface.

Table 5. The water quality of feed and permeate of different NF membranes.

	TOC (mg/L)	Ca^{2+} (mg/L)	Mg^{2+} (mg/L)	Na^{+} (mg/L)	Conductivity (μs/cm)
Feed	23.4 ± 2.6	22.6 ± 3.1	4.6 ± 1.2	73.3 ± 4.2	835.4 ± 15.1
Permeate					
NF 270	3.16 ± 1.0	6.46 ± 1.9	0.32 ± 0.1	46.78 ± 3.7	498.1 ± 10.4
cLBL	3.03 ± 0.8	5.59 ± 1.8	0.26 ± 0.1	45.84 ± 3.1	494.9 ± 9.7
LBL-cPP	2.20 ± 0.9	5.23 ± 1.6	0.20 ± 0.1	43.67 ± 3.2	480.2 ± 12.9

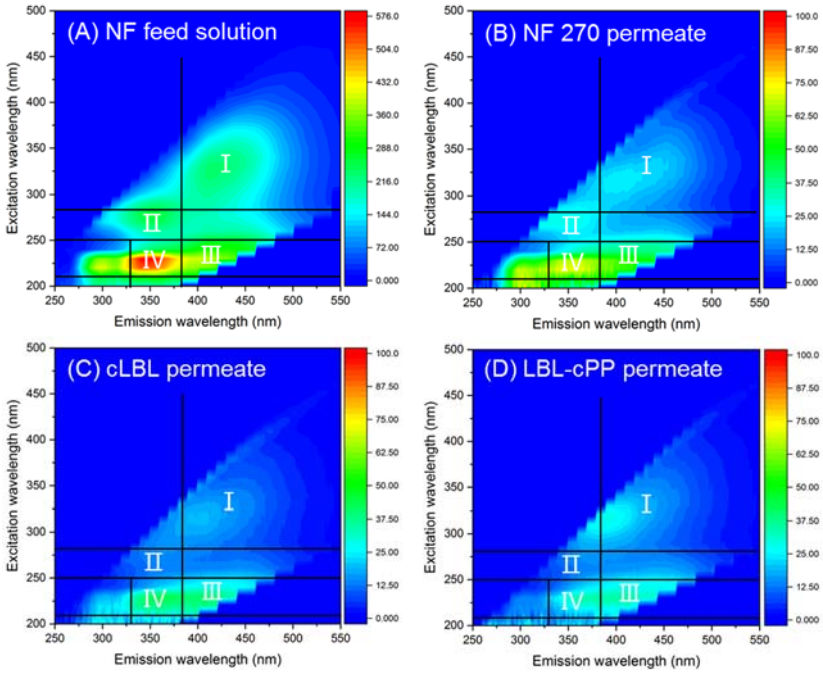

Fig. 10. EEM spectroscopy for (A) feed solution, (B) NF 270 permeate, (C) cLBL permeate, and (D) LBL-cPP permeate.

The LC-OCD as a size-exclusion chromatography was employed to further analyze the organic fractions in the feed, surface foulants and permeate of all NF processes as shown in Table 6. The contribution ratio of each organic fraction to the dissolved organic carbons (DOCs) is presented in Fig. 11. The biopolymer fraction (MW~20−100 kDa), accounting for ~23% of the total DOC in the feed, was effectively removed by all NF membranes (> 99.0%). Similarly, most of building blocks (MW~300−500 Da), as the least component (~22%) of feed solution, were also significantly removed (all > 97.7%), even though its molecular weight was close to the MWCO of selected NF membranes, which was ascribed to the retention of the formed cake layer on the membrane surface. It should be noted that less DOC (0.39 mg/L), especially for LMW (MW < 350 Da) (0.18 mg/L), was detected in the permeate of the LBL-cPP membrane than other NF membranes (Table 6). This result was also confirmed by the LC-OCD chromatogram of the LBL-cPP membrane, in which weak peaks were detected for the entire retention time along with extremely weak peak after the retention time for LMW neutrals (Fig. 12(A)), indicating its strong removal ability for organics with low molecular weight. LMW neutrals consist of weakly charged compounds such as alcohols, aldehydes, ketones and amino acids, which had been considered as the main organic foulant components on RO membrane applications [52, 53]. As the major part

(~28%) of organics in the feed solution, the efficient removal of LMW by the LBL-cPP membrane would be beneficial in controlling subsequent RO fouling. This seems in agreement with the previous results of EEM, which indicated that fulvic acid-like substances could be detected with low concentration in the permeate of LBL-cPP.

Table 6. Concentrations of dissolved organic fractions in the feed, permeate and foulant of different NF processes.

	DOC	Biopolymers	Humic substances	Building blocks	LMW
Feed (mg/L)	12.10	2.28	2.65	2.15	2.70
Permeate (mg/L)					
NF 270	0.83	0.013	N.D.	0.05	0.41
cLBL	0.51	0.009	N.D.	0.05	0.21
LBL-cPP	0.39	0.006	N.D.	0.04	0.18
Foulant (mg/m^2)					
NF 270	105.36	60.16	N.D.	13.54	12.87
cLBL	114.75	57.15	N.D.	11.68	19.55
LBL-cPP	105.06	41.23	N.D.	4.64	38.93

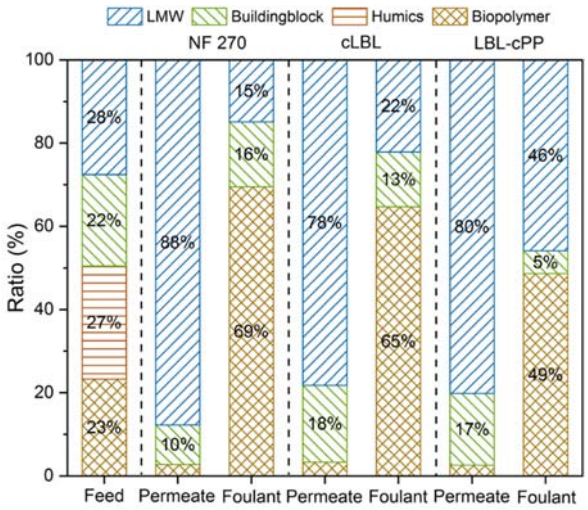

Fig. 11. Contribution ratios of dissolved organic fractions in feed, permeate and foulant of NF 270, cLBL and LBL-cPP membranes.

In NF 270, the biopolymer appeared to be the major component (69% or 60.16 mg/m^2) of the foulants owing to the high removal ability of the NF membrane for large molecular weight biopolymers. Strikingly, humic substance (MW~1000 Da), as the second abundant organic fractions (~27%) in the feed solution, were non-detected in the NF foulants. The possible reason is the transformation of smaller organic molecules to larger biopolymers through aggregation or bio-conversion [53]. Accordingly, for the LBL-cPP membrane, the foulants were consisted of 49% biopolymers (41.23 mg/m^2), 46% LMW (38.93 mg/m^2) and 5% building blocks (4.64 mg/m^2). Comparing the organic fractions ratio in the foulants of the NF 270 and cLBL membranes, it was noticed that the accretion of biopolymers on the LBL-cPP membrane surface was reduced, while the tendency of LMW presented the opposite result, which was also confirmed by the LC-OCD chromatogram of surface foulants for all NF membranes (Fig. 12 (B)). As discussed previously, the hydrophilic selective layer of the LBL-cPP NF membrane prevented the deposition of organic foulants with larger molecular weight, such as biopolymers and humic substances. Meanwhile, due to its smaller MWCO and relatively rougher surface, organic foulants with lower molecular weight, such as LMW, were partially obstructed on the membrane surface, which improved the overall permeate quality of NF membrane. In spite of this, low flux drop and reduced cleaning frequency were maintained for the LBL-cPP NF membrane (Fig. 8), suggesting it a promising candidate for treating municipal wastewater prior to the RO process.

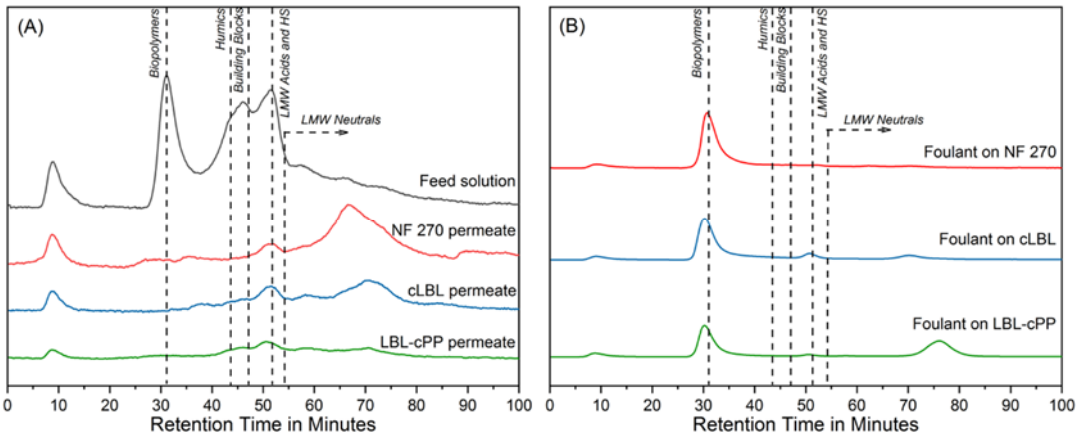

Fig. 12. The LC-OCD of organic for (A) permeate and (B) foulant of NF 270, cLBL and LBL-cPP membranes.

3.6 RO performance

After the operation of the NF process, the permeates of the NF 270, cLBL and LBL-cPP membranes were collected and directly fed to the respective RO systems to evaluate the RO performance. As shown in Fig. 13, the permeate of NF 270 caused more obvious RO membrane fouling, which induced the around 50% loss in flux after 14 days operation. This flux drop could be attributed to the following reasons: (i) Organic-inorganic fouling. As shown in Table 5, NF 270 membrane presented an undesirable Ca^{2+} rejection (~71.4%). The remaining Ca^{2+} in the NF 270 permeate may trigger the formation of bridged foulant molecules in a long-chain form, thereby exacerbating fouling [31]; (ii) Biofouling. The limited removal ability for LMW was also confirmed for NF 270 membrane (Table 6). The LMW in the RO feed could be applied by bacteria as preferred carbon source, which induced the growth of bacteria on RO membrane surface [52]. Comparatively, a lower flux drop was observed for the LBL-cPP fed RO membrane, deriving from the superior permeate quality with fewer divalent ions and dissolved organics (Table 5 and Table 6). The lower fouling tendency could translate into energy saving and operation cost saving (*e.g.* chemical cleaning) associated with fouling [18].

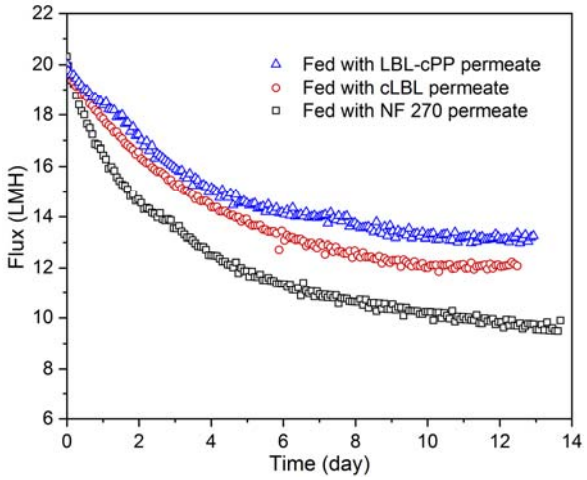

Fig. 13. Flux profiles of the RO system fed with permeate from NF 270, cLBL and LBL-cPP.

4. Conclusions

A novel low-pressure NF membrane was successfully fabricated on the polyelectrolyte LBL assembled PES substrate via $H_2O_2/CuSO_4$ triggered co-deposition of PDA/PEI followed by GA crosslinking. A homogeneous surface with fewer PDA aggregates was tailored based on the synergetic covalent effects of PDA with PEI and LBL components, conferring the NF membrane

with outstanding hydrophilicity of 22.5° and slightly positive charged coating with an isoelectric point of pH 6.8. The novel NF membrane presented desirable pure water permeability and satisfactory divalent cations rejection under 2 bar, which was competitive to those previously reported NF membranes. It also remained robust after long-term pure water filtration and acidic/alkaline treatment. Significantly, the PDA/PEI modified low-pressure NF membrane achieved higher organic and inorganic removal with limited flux reduction, reduced cleaning frequency and controlled foulant adhesion during the practical filtration process with municipal wastewater. The subsequent RO process fed with the permeate from this novel NF membrane displayed better performance due to its improved water quality. With the acquisition of high separation performance, structural stability and fouling resistance, the PDA/PEI modified low-pressure NF membrane is a potential candidate for energy-efficient and low-cost water reclamation.

Acknowledgements

This research grant was supported by the Singapore National Research Foundation under its Environment and Water Research Program and administered by PUB, Singapore's National Water Agency. The Singapore Membrane Technology Center, Nanyang Environment and Water Research Institute, Nanyang Technological University is supported by the Economic Development Board of Singapore.

References

[1] J. Eliasson, The rising pressure of global water shortages, Nature News, 517 (2015) 6.

[2] J.R. Werber, C.O. Osuji, M. Elimelech, Materials for next-generation desalination and water purification membranes, Nat. Rev. Mater., 1 (2016) 16018.

[3] P. Phungsai, F. Kurisu, I. Kasuga, H. Furumai, Molecular characterization of low molecular weight dissolved organic matter in water reclamation processes using Orbitrap mass spectrometry, Water Res., 100 (2016) 526-536.

[4] W. Luo, H.V. Phan, M. Xie, F.I. Hai, W.E. Price, M. Elimelech, L.D. Nghiem, Osmotic versus conventional membrane bioreactors integrated with reverse osmosis for water reuse: Biological stability, membrane fouling, and contaminant removal, Water Res., 109 (2017) 122-134.

[5] K. Kimura, S. Okazaki, T. Ohashi, Y. Watanabe, Importance of the co-presence of silica and organic matter in membrane fouling for RO filtering MBR effluent, J. Membr. Sci., 501 (2016) 60-67.

[6] P. Krzeminski, L. Leverette, S. Malamis, E. Katsou, Membrane bioreactors – A review on recent developments in energy reduction, fouling control, novel configurations, LCA and market prospects, J. Membr. Sci., 527 (2017) 207-227.

[7] L.N. Sim, T.H. Chong, A.H. Taheri, S.T.V. Sim, L. Lai, W.B. Krantz, A.G. Fane, A review of fouling indices and monitoring techniques for reverse osmosis, Desalination, 434 (2018) 169-188.

[8] F.C. Kent, K. Farahbakhsh, B. Mahendran, M. Jaklewicz, S.N. Liss, H. Zhou, Water reclamation using reverse osmosis: Analysis of fouling propagation given tertiary membrane filtration and MBR pretreatments, J. Membr. Sci., 382 (2011) 328-338.

[9] J.-H. Choi, S. Dockko, K. Fukushi, K. Yamamoto, A novel application of a submerged nanofiltration membrane bioreactor (NF MBR) for wastewater treatment, Desalination, 146 (2002) 413-420.

[10] J. Mamo, S. Insa, H. Monclús, I. Rodríguez-Roda, J. Comas, D. Barceló, M.J. Farré, Fate of NDMA precursors through an MBR-NF pilot plant for urban wastewater reclamation and the effect of changing aeration conditions, Water Res., 102 (2016) 383-393.

[11] M.L. Bruening, D.M. Dotzauer, P. Jain, L. Ouyang, G.L. Baker, Creation of functional membranes using polyelectrolyte multilayers and polymer brushes, Langmuir, 24 (2008) 7663-7673.

[12] S. Rajabzadeh, C. Liu, L. Shi, R. Wang, Preparation of low-pressure water softening hollow fiber membranes by polyelectrolyte deposition with two bilayers, Desalination, 344 (2014) 64-70.

[13] N. Dizge, R. Epsztein, W. Cheng, C.J. Porter, M. Elimelech, Biocatalytic and salt selective multilayer polyelectrolyte nanofiltration membrane, J. Membr. Sci., 549 (2018) 357-365.

[14] G.-R. Xu, S.-H. Wang, H.-L. Zhao, S.-B. Wu, J.-M. Xu, L. Li, X.-Y. Liu, Layer-by-layer (LBL) assembly technology as promising strategy for tailoring pressure-driven desalination membranes, J. Membr. Sci., 493 (2015) 428-443.

[15] M. Kolasinska, R. Krastev, T. Gutberlet, P. Warszynski, Layer-by-layer deposition of polyelectrolytes. Dipping versus spraying, Langmuir, 25 (2008) 1224-1232.

[16] P. Bertrand, A. Jonas, A. Laschewsky, R. Legras, Ultrathin polymer coatings by complexation

of polyelectrolytes at interfaces: suitable materials, structure and properties, Macromol. Rapid Comm., 21 (2000) 319-348.

[17] C. Liu, L. Shi, R. Wang, Crosslinked layer-by-layer polyelectrolyte nanofiltration hollow fiber membrane for low-pressure water softening with the presence of SO_4^{2-} in feed water, J. Membr. Sci., 486 (2015) 169-176.

[18] M.F. Tay, C. Liu, E.R. Cornelissen, B. Wu, T.H. Chong, The feasibility of nanofiltration membrane bioreactor (NF-MBR)+reverse osmosis (RO) process for water reclamation: Comparison with ultrafiltration membrane bioreactor (UF-MBR)+RO process, Water Res., 129 (2018) 180-189.

[19] K. Itano, J. Choi, M.F. Rubner, Mechanism of the pH-induced discontinuous swelling/deswelling transitions of poly (allylamine hydrochloride)-containing polyelectrolyte multilayer films, Macromolecules, 38 (2005) 3450-3460.

[20] X. Shi, G. Tal, N.P. Hankins, V. Gitis, Fouling and cleaning of ultrafiltration membranes: A review, J. Water Process Eng., 1 (2014) 121-138.

[21] C. Regula, E. Carretier, Y. Wyart, G. Gésan-Guiziou, A. Vincent, D. Boudot, P. Moulin, Chemical cleaning/disinfection and ageing of organic UF membranes: A review, Water Res., 56 (2014) 325-365.

[22] H.-C. Yang, J. Luo, Y. Lv, P. Shen, Z.-K. Xu, Surface engineering of polymer membranes via mussel-inspired chemistry, J. Membr. Sci., 483 (2015) 42-59.

[23] W.-Z. Qiu, H.-C. Yang, Z.-K. Xu, Dopamine-assisted co-deposition: An emerging and promising strategy for surface modification, Adv. Colloid Interface Sci., 256 (2018) 111-125.

[24] N.G.P. Chew, S. Zhao, C. Malde, R. Wang, Superoleophobic surface modification for robust membrane distillation performance, J. Membr. Sci., 541 (2017) 162-173.

[25] N.G.P. Chew, S. Zhao, C. Malde, R. Wang, Polyvinylidene fluoride membrane modification via oxidant-induced dopamine polymerization for sustainable direct-contact membrane distillation, J. Membr. Sci., 563 (2018) 31-42.

[26] H.C. Yang, R.Z. Waldman, M.B. Wu, J. Hou, L. Chen, S.B. Darling, Z.K. Xu, Dopamine: Just the Right Medicine for Membranes, Adv. Funct. Mater., 28 (2018) 1705327.

[27] J. Wang, J. Zhu, M.T. Tsehaye, J. Li, G. Dong, S. Yuan, X. Li, Y. Zhang, J. Liu, B. Van der Bruggen, High flux electroneutral loose nanofiltration membranes based on rapid deposition of

polydopamine/polyethyleneimine, J. Mater. Chem. A, 5 (2017) 14847-14857.

[28] C. Zhang, H.-N. Li, Y. Du, M.-Q. Ma, Z.-K. Xu, $CuSO_4/H_2O_2$-triggered polydopamine/poly (sulfobetaine methacrylate) coatings for antifouling membrane surfaces, Langmuir, 33 (2017) 1210-1216.

[29] Y.-N. Wang, J. Wei, Q. She, F. Pacheco, C.Y. Tang, Microscopic characterization of FO/PRO membranes–a comparative study of CLSM, TEM and SEM, Environ. Sci. Technol., 46 (2012) 9995-10003.

[30] B. Wu, T. Kitade, T.H. Chong, T. Uemura, A.G. Fane, Impact of membrane bioreactor operating conditions on fouling behavior of reverse osmosis membranes in MBR–RO processes, Desalination, 311 (2013) 37-45.

[31] X. Li, J. Li, X. Fang, K. Bakzhan, L. Wang, B. Van der Bruggen, A synergetic analysis method for antifouling behavior investigation on PES ultrafiltration membrane with self-assembled TiO_2 nanoparticles, J. Colloid Interf. Sci., 469 (2016) 164-176.

[32] Y. Liu, K. Ai, L. Lu, Polydopamine and its derivative materials: synthesis and promising applications in energy, environmental, and biomedical fields, Chem. Rev., 114 (2014) 5057-5115.

[33] N.F. Della Vecchia, R. Avolio, M. Alfè, M.E. Errico, A. Napolitano, M. d'Ischia, Building‐block diversity in polydopamine underpins a multifunctional eumelanin‐type platform tunable through a quinone control point, Adv. Func. Mater., 23 (2013) 1331-1340.

[34] M. Mateescu, M.-H. Metz-Boutigue, P. Bertani, V. Ball, Polyelectrolytes to produce nanosized polydopamine, J. Colloid Interf. Sci., 469 (2016) 184-190.

[35] C. Liu, W. Fang, S. Chou, L. Shi, A.G. Fane, R. Wang, Fabrication of layer-by-layer assembled FO hollow fiber membranes and their performances using low concentration draw solutions, Desalination, 308 (2013) 147-153.

[36] Y.-L. Ji, M.B.M.Y. Ang, H.-C. Hung, S.-H. Huang, Q.-F. An, K.-R. Lee, J.-Y. Lai, Bio-inspired deposition of polydopamine on PVDF followed by interfacial cross-linking with trimesoyl chloride as means of preparing composite membranes for isopropanol dehydration, J. Membr. Sci., 557 (2018) 58-66.

[37] Y. Xu, Y. Lin, N.G.P. Chew, C. Malde, R. Wang, Biocatalytic PVDF composite hollow fiber membranes for CO_2 removal in gas-liquid membrane contactor, J. Membr. Sci., 572 (2019) 532-544.

[38] Z.-Y. Xi, Y.-Y. Xu, L.-P. Zhu, Y. Wang, B.-K. Zhu, A facile method of surface modification for hydrophobic polymer membranes based on the adhesive behavior of poly (DOPA) and poly (dopamine), J. Membr. Sci., 327 (2009) 244-253.

[39] L. Ouyang, R. Malaisamy, M.L. Bruening, Multilayer polyelectrolyte films as nanofiltration membranes for separating monovalent and divalent cations, J. Membr. Sci., 310 (2008) 76-84.

[40] N. Wang, S. Ji, G. Zhang, J. Li, L. Wang, Self-assembly of graphene oxide and polyelectrolyte complex nanohybrid membranes for nanofiltration and pervaporation, Chem. Eng. J., 213 (2012) 318-329.

[41] L. Wang, N. Wang, J. Li, J. Li, W. Bian, S. Ji, Layer-by-layer self-assembly of polycation/GO nanofiltration membrane with enhanced stability and fouling resistance, Sep. Purif. Technol., 160 (2016) 123-131.

[42] Q. Nan, P. Li, B. Cao, Fabrication of positively charged nanofiltration membrane via the layer-by-layer assembly of graphene oxide and polyethylenimine for desalination, Appl. Surf. Sci., 387 (2016) 521-528.

[43] Y. Zhang, S. Zhang, J. Gao, T.-S. Chung, Layer-by-layer construction of graphene oxide (GO) framework composite membranes for highly efficient heavy metal removal, J. Membr. Sci., 515 (2016) 230-237.

[44] Y. Lv, Y. Du, W.-Z. Qiu, Z.-K. Xu, Nanocomposite membranes via the codeposition of polydopamine/polyethylenimine with silica nanoparticles for enhanced mechanical strength and high water permeability, ACS Appl. Mater. Interfaces, 9 (2017) 2966-2972.

[45] N. Meng, W. Zhao, E. Shamsaei, G. Wang, X. Zeng, X. Lin, T. Xu, H. Wang, X. Zhang, A low-pressure GO nanofiltration membrane crosslinked via ethylenediamine, J. Membr. Sci., 548 (2018) 363-371.

[46] Y. Huang, J. Sun, D. Wu, X. Feng, Layer-by-layer self-assembled chitosan/PAA nanofiltration membranes, Sep. Purif. Technol., 207 (2018) 142-150.

[47] S. Hong, Y.S. Na, S. Choi, I.T. Song, W.Y. Kim, H. Lee, Non-covalent self-assembly and covalent polymerization co-contribute to polydopamine formation, Adv. Func. Mater., 22 (2012) 4711-4717.

[48] H. Wei, J. Ren, B. Han, L. Xu, L. Han, L. Jia, Stability of polydopamine and poly (DOPA) melanin-like films on the surface of polymer membranes under strongly acidic and alkaline

conditions, Colloids Surf. B: Biointerfaces, 110 (2013) 22-28.

[49] C.C. Chang, K.W. Kolewe, Y. Li, I. Kosif, B.D. Freeman, K.R. Carter, J.D. Schiffman, T. Emrick, Underwater superoleophobic surfaces prepared from polymer zwitterion/dopamine composite coatings, Adv. Mater. Interfaces, 3 (2016) 1500521-1500529.

[50] A. Antony, J.H. Low, S. Gray, A.E. Childress, P. Le-Clech, G. Leslie, Scale formation and control in high pressure membrane water treatment systems: a review, J. Membr. Sci., 383 (2011) 1-16.

[51] L.H. Kim, T.H. Chong, Physiological responses of salinity-stressed *vibrio* sp. and the effect on the biofilm formation on a nanofiltration membrane, Environ. Sci. Technol., 51 (2017) 1249-1258.

[52] S. Jeong, G. Naidu, R. Vollprecht, T. Leiknes, S. Vigneswaran, In-depth analyses of organic matters in a full-scale seawater desalination plant and an autopsy of reverse osmosis membrane, Sep. Purif. Technol., 162 (2016) 171-179.

[53] T. Fujioka, H. Kodamatani, H. Aizawa, S. Gray, K.P. Ishida, L.D. Nghiem, Role of membrane fouling substances on the rejection of *N*-nitrosamines by reverse osmosis, Water Res., 118 (2017) 187-195.

Appendix A.

Fig. A1

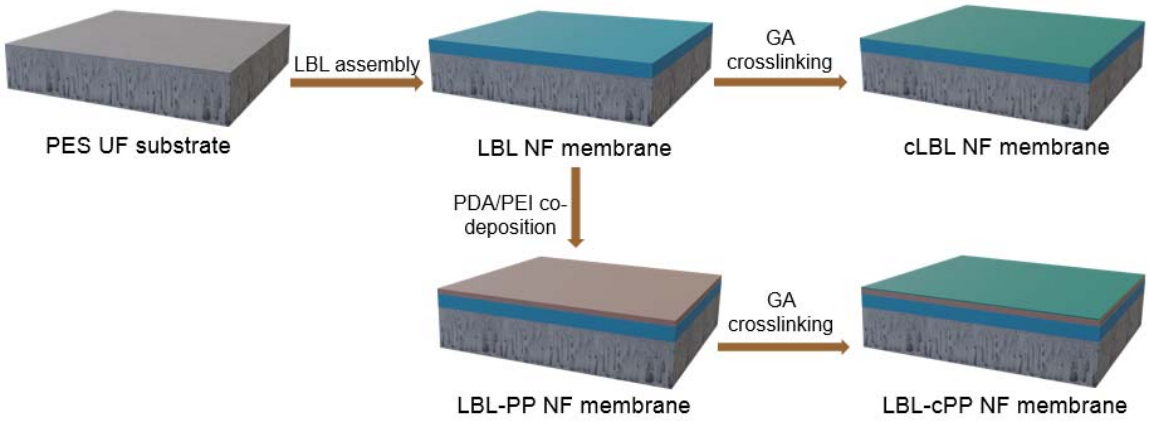

Fig. A1. The scheme of fabrication procedure for different NF membranes.

Fig. A2

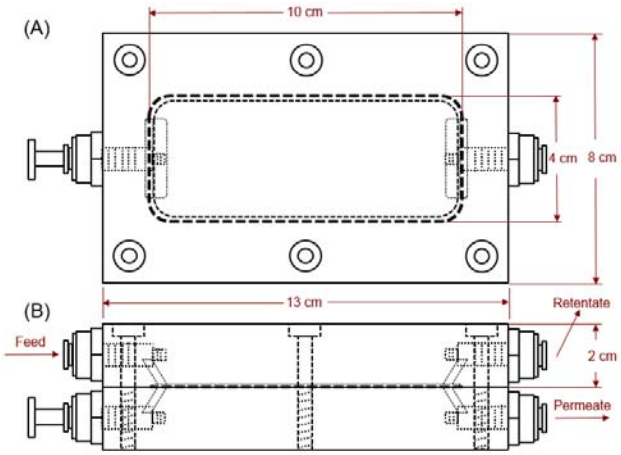

Fig. A2. The scheme of membrane cell from (A) front view and (B) side view with main dimension (Gap height: 1 mm).

Fig. A3

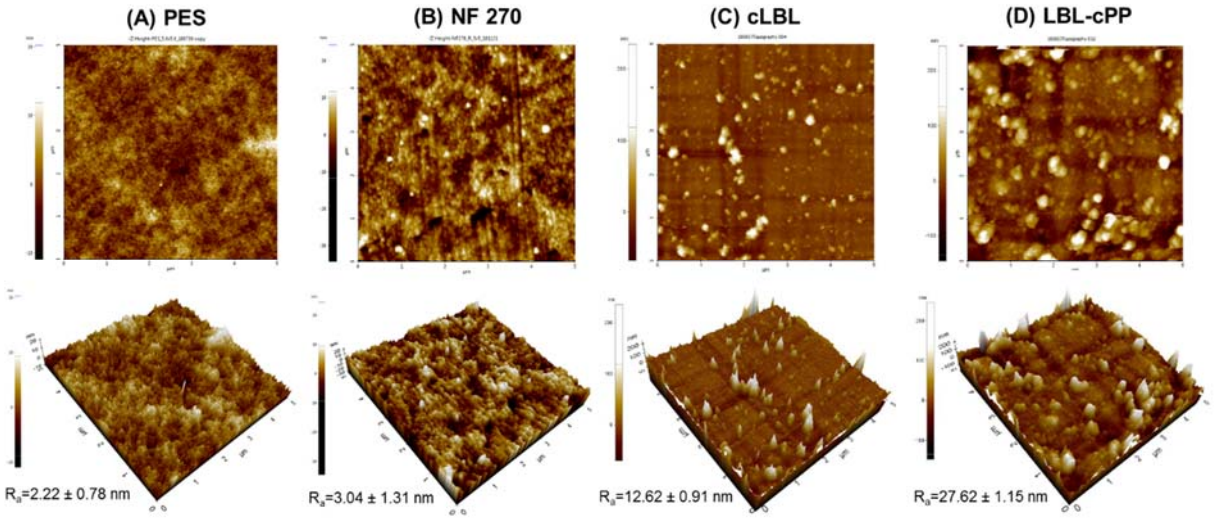

Fig. A3. AFM images for (A) PES substrate, (B) NF 270, (C) cLBL, and (D) LBL-cPP membranes.

Table A1

Table A1. The permeability and separation performances of LBL and LBL-PP NF membranes [a]

	Pure water permeability (LMH/bar)	NaCl		Na_2SO_4		$MgSO_4$		$MgCl_2$	
		Permeability (LMH/bar)	Rejection (%)	Permeability (LMH/bar)	Rejection (%)	Permeability (LMH/bar)	Rejection (%)	Permeability (LMH/bar)	Rejection (%)
LBL	14.7 ± 1.2	12.9 ± 0.6	10.6 ± 0.4	11.4 ± 0.4	37.4 ± 0.2	9.9 ± 0.5	71.5 ± 0.3	7.4 ± 0.4	82.4 ± 0.3
LBL-PP	11.2 ± 1.1	10.5 ± 0.6	17.5 ± 0.6	9.2 ± 0.5	57.8 ± 0.5	8.4 ± 0.6	79.1 ± 0.2	7.1 ± 0.3	87.3 ± 0.4

[a] Experimental conditions: salt concentration, 1000 ppm; crossflow velocity, 0.3 m/s; pH 6; operation pressure, 2 bar; temperature, 25 ± 0.5 °C.

Fig. A4

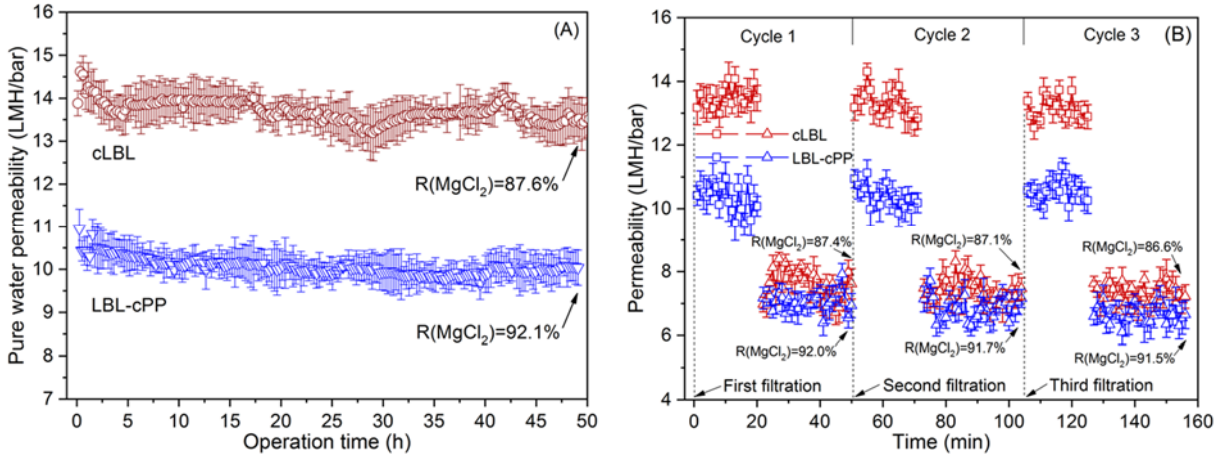

Fig. A4. Stability test of NF membranes with (A) pure water (2 bar, 25 ± 0.5 °C) and (B) acidic solution (Test procedure and conditions for each cycle: acidic treatment (1h without pressure) -> pure water permeability test (20 h, 2 bar, presented as squares) -> $MgCl_2$ rejection test (30 h, 2 bar, presented as triangles)). For acidic treatment test, the original permeability and $MgCl_2$ rejection for cLBL and LBL-cPP membranes were 13.2 LMH/bar, 88.4% and 10.7 LMH/bar, 93.8 %, respectively.

Fig. A5

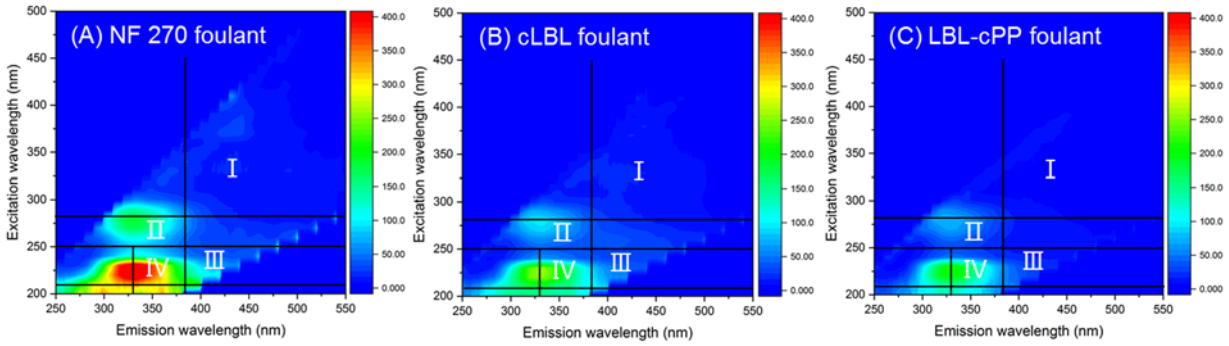

Fig. A5. EEM spectroscopy for the foulants on (A) NF 270, (B) cLBL and (C) LBL-cPP membranes.